

RESEARCH ARTICLE | NOVEMBER 13 2023

Electromechanical analysis of electrospun polymer fiber deposition

Ka Chun Chan ; Ahsana Sadaf; Jan Gerrit Korvink ; Wolfgang Wenzel  

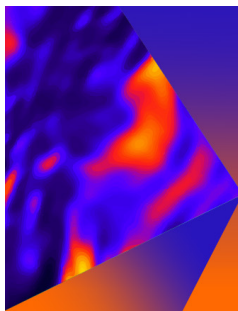


J. Appl. Phys. 134, 184902 (2023)

<https://doi.org/10.1063/5.0171903>



CrossMark



Applied Physics Letters

Special Topic: Mid and Long Wavelength Infrared Photonics, Materials, and Devices

Submit Today



Electromechanical analysis of electrospun polymer fiber deposition

Cite as: J. Appl. Phys. **134**, 184902 (2023); doi: [10.1063/5.0171903](https://doi.org/10.1063/5.0171903)

Submitted: 11 August 2023 · Accepted: 21 October 2023 ·

Published Online: 13 November 2023



View Online



Export Citation



CrossMark

Ka Chun Chan,¹  Ahsana Sadaf,² Jan Gerrit Korvink,²  and Wolfgang Wenzel^{1,a)} 

AFFILIATIONS

¹Institute of Nanotechnology (INT), Karlsruhe Institute of Technology (KIT), Hermann-von-Helmholtz Platz 1, Eggenstein-Leopoldshafen 76344, Germany

²Institute of Microstructure Technology (IMT), Karlsruhe Institute of Technology (KIT), Hermann-von-Helmholtz Platz 1, Eggenstein-Leopoldshafen 76344, Germany

^{a)}Author to whom correspondence should be addressed: wolfgang.wenzel@kit.edu

ABSTRACT

Electrospinning is an important technique to fabricate nanofibers. In recent years, near-field electrospinning (NFES) has been developed to enhance the control of nanofiber deposition compared to conventional electrospinning, achieved by reducing the operating distance and electric field. This enables the construction of high-aspect ratio 3D structures in a self-aligned, layer-by-layer manner. However, the alignment of fiber deposition can be hindered by charge accumulation in the polymer fibers. Furthermore, a theoretical understanding of the underlying fiber deposition mechanism is still lacking. Herein, we present a numerical model for studying the charge transport, dissipation, and accumulation of NFES polymer fiber deposition. The model reveals that the presence of a trapped state in polymeric materials imposes limitations on the quality of charged fiber deposition. Moreover, the effect of different substrate materials on charge dissipation in fiber deposition is studied. To validate the model, we compare the simulation results with NFES experiments, demonstrating qualitative agreement. We also analyze the effect of the fiber materials and experimental parameters on the printing quality. This model provides an approach to analyze and optimize the operating parameters of NFES to achieve precise and stable nanofiber deposition.

© 2023 Author(s). All article content, except where otherwise noted, is licensed under a Creative Commons Attribution (CC BY) license (<http://creativecommons.org/licenses/by/4.0/>). <https://doi.org/10.1063/5.0171903>

I. INTRODUCTION

Nanoscale additive manufacturing (AM) is a method of fabricating complex nanoscale structures via self-assembly or directed assembly.^{1–4} AM has greater flexibility and programmability than conventional manufacturing methods for fabricating complex structural architectures.⁵ As a result, it has gained huge popularity in a variety of fields, i.e., sensors,^{6,7} energy devices,^{8,9} and biomedical applications.^{10–12} There are various additive nanomanufacturing technologies, such as e-beam lithography,¹³ direct laser writing,¹⁴ and direct ink writing.¹⁵ Each technology has its own set of characteristics, benefits, and drawbacks. Lithography-based technologies, for example, have a high printing resolution,¹⁴ but they are constrained by slow manufacturing speed, high infrastructure costs, and reliance on epoxy-based polymer inks. The flow-based ink printing technologies, on the other hand, are more efficient and require less infrastructure costs, but the printing resolution is

relatively low.¹⁶ Among the available technologies, near-field electrospinning (NFES) shows advantages in terms of resolution, printing speed, and material processing, allowing rapid, scalable, and flexible fabrication of complex 3D structures with programmable properties.

Electrospinning is a continuous nanofiber production method driven by an electric field between a metallic nozzle and a grounded substrate.^{17,18} The electric charges induced by the electric field accumulate on the surface of the liquid droplet. The electric force acting on the charged droplet, which pulls it toward the substrate, competes with surface tension, causing it to form a conical shape, known as the Taylor cone.¹⁹ When the electric force exceeds the surface tension, the droplet's surface breaks and ejects the electrified thin jet. For conventional electrospinning, the operating distance between the nozzle and the substrate is large. Therefore, the electrified jet whips due to a bending instability, resulting in inaccurate nanofiber deposition.²⁰ There are several works to investigate

31 January 2024 16:30:28

the flow properties of the electrified jets²¹ and modifications, such as orthogonal rotating electric fields²² and controlled gas flow,²³ have been explored to study the bending instabilities and radius of the electrified polymer jets. Near-field electrospinning is one of the approaches that has been developed to improve the controllability of the electrospun fiber collections, achieved by shortening the operating distance and reducing the applied electric field.^{24,25} As a result, the nanofibers can be precisely controlled by depositing them before the initiation of whipping motion.

As a nanoscale AM method, NFES can print at a high speed (>20 cm/s) with a high resolution (<100 nm) and is also applicable to a wide range of materials, i.e., polymers,^{26,27} carbon,^{28,29} and metal oxides.^{30,31} However, one of the major limitations of NFES is the charge accumulation in the deposited fibers. During the fiber deposition, in-flight fibers deposit on top of the deposited fibers in a self-aligned manner.^{32–34} This enables stacking the nanofiber consistently to form a high aspect ratio structure. When the charge dissipation is slow, the residual charges accumulate in the deposited structure. As a result, the electric repulsion between the fibers limit the self-alignment of the fibers. Several studies have been conducted to analyze and improve the charge dissipation of the charged fibers. Catalani *et al.* found that the residual charge is trapped within the crystalline phase due to molecular orientation.³⁵ Park *et al.* demonstrated that the charge dissipation can be enhanced by adding sodium chloride into the polymer solution, which enables fabricating 3D wall structures with a high-aspect ratio.³⁶ Sadaf *et al.* investigated the effect of different substrates on NFES and found that the conductor substrate outperforms all other candidates.³⁷ However, a theoretical model of the charge dissipation mechanism of NFES fiber deposition is still lacking.

In this work, we develop a model for the charge transport in the dielectric medium for the NFES fiber deposition. We consider a one-dimensional charge transport model in a dielectric material subjected to an external electric field,³⁸ in which charge is transferred from the deposited fiber to the grounded substrate. Dielectric charge transport models have been employed to study the dynamics of space charges in various dielectric materials, e.g., charge injection in dielectric thin film,³⁹ polyethylene,⁴⁰ and space charge accumulation in high voltage cable.^{41,42} Herein, we will study the space charge dynamics in the deposited fiber and demonstrate that THE trapped state is the main source of slow charge dissipation. Furthermore, the effect of various substrates on the charge dissipation will be demonstrated.

The paper is organized as follows. The one-dimensional charge transport model is introduced in Sec. II. The results of space charge dynamics in the dielectric deposited fibers and the electro-mechanical behavior of the NFES fiber deposition are presented and discussed in Sec. III. The paper concludes in Sec. IV with a summary of the key results.

II. METHOD

A. Charge transport model

In this section, we develop a charge transport model of charged polymer fiber deposition for NFES. Figure 1(a) shows the schematic diagram of NFES fiber deposition. In the direct-writing NFES, an electric potential Φ is applied between a nozzle and a

substrate over a distance L such that the induced charge in the polymer droplet is ejected from the Taylor cone and carried by the ejecting jet. The electrified jet deposits on a rotating grounded substrate at rotational speed ω in a fiber-by-fiber manner, forming a stacked wall structure via the self-alignment mechanism. The residual charges in the polymer fiber are transported from the fiber to the grounded substrate by the external electric field. Due to the symmetry along the radial direction, we assume that the charge transport occurs only along the vertical z -direction and employ a one-dimensional model.

We consider a 1D fiber with infinitesimal small width dx and height h , which is stacked on top of the deposited fiber wall for each deposition time t_d . The charge distribution of the 1D fiber is described by a Gaussian distribution,

$$\rho(z) = \rho_0 e^{-\frac{1}{2}\left(\frac{z-(h-w)}{\sigma}\right)^2}, \quad (1)$$

where ρ_0 is a charge constant that determines the charge density of the fiber and w and σ are the width and standard deviation of the Gaussian distribution, respectively.

Bipolar charge transport is commonly considered in the dielectric charge transport model,³⁸ as both positive and negative charges are generated in dielectric materials. However, only one of the charge carriers is dominant in the electrified jet of NFES. Therefore, we consider the positive charge as the only charge carrier in our model, and its dynamics in the deposited fibers are described by the following set of coupled equations.

(1) Transport equation,

$$J(z, t) = \mu E(z, t)\rho(z, t) - D\nabla\rho(z, t). \quad (2)$$

(2) Continuity equation,

$$\frac{\partial J(z, t)}{\partial z} + \frac{\partial \rho(z, t)}{\partial t} = 0. \quad (3)$$

(3) Poisson equation,

$$\frac{\partial E(z, t)}{\partial z} = \frac{\rho(z, t)}{\epsilon\epsilon_0}, \quad (4)$$

where J is the transport current, E is the electric field strength, ρ is the charge density, μ is the mobility of the charge carriers, D is the diffusivity of the charge carriers, ϵ is the dielectric constant, and ϵ_0 is the permittivity of vacuum. On the right-hand side of Eq. (2), the first term is the drift flux, and the second term is the diffusion flux.

Charges can be stored in the trapped states of polymeric materials for a long time,⁴³ as shown in Fig. 1(b). These trapped states depend on crystallinity,⁴⁴ polymer structure,⁴⁵ and the presence of additives.⁴⁶ To introduce the trapped and mobile states into the model, the total charge density is rewritten as the sum of them,

$$\rho = \rho_t + \rho_f, \quad (5)$$

where ρ_t is the charge density in the trapped states and ρ_f is the charge density in the mobile states. Moreover, the source terms for

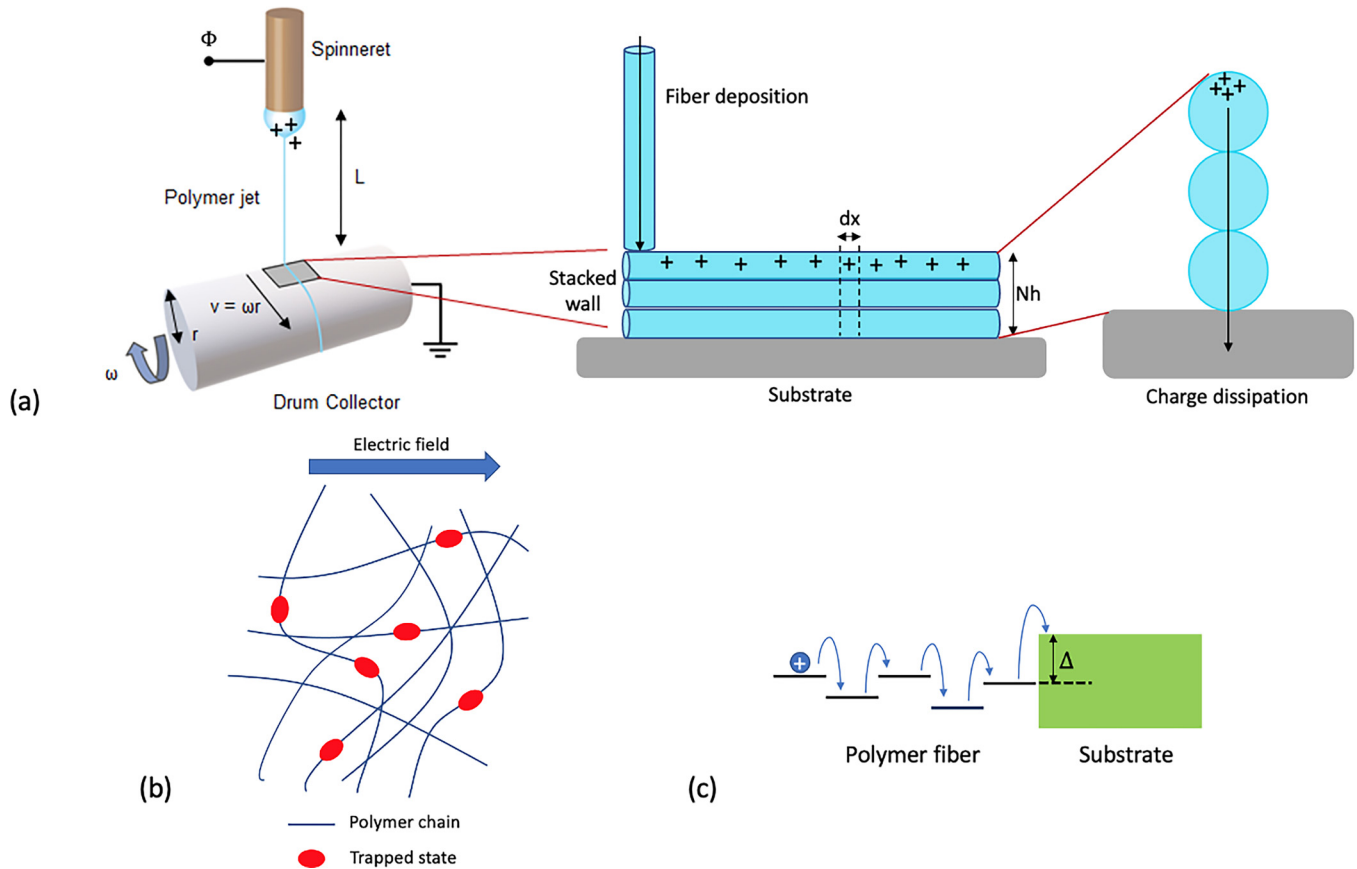


FIG. 1. (a) Schematic diagram of the electrospinning setup in which the charges in the polymer fiber are transported from the top of the wall structure down to the substrate. Adapted with permission from A. Sadaf, *Adv. Eng. Mater.* **24**, 2101740 (2022). Copyright 2022 Author(s), licensed under a Creative Commons Attribution (CC BY) license). (b) The presence of the trapped state in polymer medium. (c) The energy barrier at the polymer fiber/substrate interface due to material mismatch.

31 January 2024 16:30:28

the trapped states and the mobile states are given by

$$S_t = R_{f \rightarrow t} \rho_f \left(1 - \frac{\rho_t}{N_t} \right) - R_{t \rightarrow f} \rho_t, \quad (6)$$

$$S_f = -R_{f \rightarrow t} \rho_f \left(1 - \frac{\rho_t}{N_t} \right) + R_{t \rightarrow f} \rho_t, \quad (7)$$

where $R_{f \rightarrow t}$ is the rate of charge transfer from the mobile state to the trapped state, $R_{t \rightarrow f}$ is the rate of charge transfer from the trapped state to the mobile state, and N_t is the density of the trapped state. As a result, the continuity equation in Eq. (3) can be separated into the trapped and mobile states,

$$\frac{\partial \rho_t(z, t)}{\partial t} = S_t, \quad (8)$$

$$\frac{\partial J(z, t)}{\partial z} + \frac{\partial \rho_f(z, t)}{\partial t} = S_f. \quad (9)$$

At the interface between the deposited fiber and the grounded substrate, the charges are transported from one material to another via a hopping mechanism in which the charges have to overcome an energy barrier, as shown in Fig. 1(c). Therefore, we propose that the boundary condition of the current at the fiber/substrate interface is given by

$$J(z = 0, t) = \mu E(0, t) \rho(0, t) \exp\left(-\frac{\Delta}{k_B T}\right), \quad (10)$$

where Δ is the energy barrier, k_B is the Boltzmann constant, and T is the temperature.

B. Experimental setup

To validate the charge transport model, we compare it with a NFES experimental setup. As illustrated in Fig. 1(a), a stainless steel needle is placed at a short distance (1–2 mm) above a rotating grounded drum, and a substrate is placed on the rotating drum to collect the depositing nanofiber so that the short distance minimizes the fiber deflection and enables layer-by-layer deposition. The drum has a diameter of 14 cm and rotates at a speed of 100 cm/s, which is equivalent to the deposition rate of 440 ms^{-1} . The drum is grounded, and a voltage of 900–1000 V is applied to the needle. Moreover, we used polyethylene oxide (PEO) as the electrospinnable polymer feedstock, with a solvent consisting of 40% methanol and 60% water. The samples of the electrospun fibers were collected by the substrate attached on the rotating drum and then the morphology and shape of the stacked walls were visualized by scanning electron microscope to analyze the quality of printing.

The model parameters are presented in Table I. To reduce the computational cost, we consider a system with a smaller operating distance, i.e., $L = 300 \mu\text{m}$, between the needle and the substrate and a rescaled voltage, i.e., $V = 187.5 \text{ V}$, in the simulation.

III. RESULTS AND DISCUSSION

In this section, we present and discuss the simulation results, as well as compare them to the experimental data. We first computed and compared the charge dynamics of the system with and without the trapped states to study the source of the charge accumulation. We then performed the charged fiber deposition simulation to show how the self-alignment mechanism works and breaks down. In addition, the effects of various substrate materials on fiber deposition are investigated.

A. Charge dissipation

In order to investigate the effect of the trapped state on charge dissipation, we compared the change of total charges inside the

deposited polymer fiber (i) without the trapped state and (ii) with the trapped state over time. At initial time $t = 0$, the charge density is described by a Gaussian distribution at the surface of the deposited fiber, as shown in Eq. (1). For the fiber without the trapped state, all charge carriers are in the mobile states, i.e., $\rho_f = \rho$ and $\rho_t = 0$. Also, the rate of charge transfer from the mobile state to the trapped state or from the trapped state to the mobile state is all zero, i.e., $R_{f \rightarrow t} = 0$ and $R_{t \rightarrow f} = 0$. For the fiber with the trapped state, we set 30% of the charge carriers in the mobile states while the remaining in the trapped states at $t = 0$, i.e., $\rho_f = 0.3\rho$ and $\rho_t = 0.7\rho$. Since the mobile charges are dissipated rapidly, the ratio of the mobile states to the trapped states goes quickly to an equilibrium state. As a result, the ratio of the trapped states to mobile states at $t = 0$ would mainly affect the initial charge density. In addition, the values of $R_{f \rightarrow t}$ and $R_{t \rightarrow f}$ are presented in Table I.

Figures 2(a) and 2(b) show the charge distribution inside the deposited fiber at $t = 0 \text{ ms}$ and $t = 440 \text{ ms}$ (i) without the trapped state and (ii) with the trapped state, respectively. At initial time $t = 0 \text{ ms}$, the charge distribution of both systems is the same. The charge distribution of the system without the trapped state drops to zero after 400 ms, whereas the charge distribution of the system with the trapped state decays but remains non-zero.

Figure 2(c) shows the results of charge dissipation in the deposited polymeric fiber over time. For the curve without the trapped state, the total charge drops rapidly to zero within 20 ms. Under an external electric field, the charges are rapidly dissipated as they can move from the fiber surface to the substrate at a high velocity without trapped. Because of the contribution of the mobile charges, the curve with the trapped state decays at nearly the same rate as the curve without the trapped state at the beginning. After a few milliseconds, the curve decays much slower because the majority of the charge carriers are in the trapped states. Therefore, the residue charge of the curve with the trapped state is non-zero after $t = 440 \text{ ms}$ and the charges accumulate.

B. The breakdown of self-alignment

We demonstrated in Sec. III A that the charge accumulation is caused by the trapped state of charge carriers within polymeric materials. In this section, we consider that a charged polymer fiber deposits on top of the deposited wall structure every 440 ms. The charge distribution in each newly deposited fiber is described by Eq. (1), with 30% of the charge carriers in the mobile states and 70% in the trapped states, i.e., $\rho_f = 0.3\rho$ and $\rho_t = 0.7\rho$. The electric field on the surface of the wall structure E_{sur} is computed over time to analyze the electromechanical properties of the charged fiber deposition. Since the in-flight polymer fiber is positively charged, a negative value of the surface E-field indicates the attractive interaction between the in-flight fiber and the deposited fibers, whereas a positive value indicates the repulsive interaction.

The charge distribution inside the wall structure at $t = 2200 \text{ ms}$, just before the deposition of the fifth layer, is depicted in Fig. 3(a). The charges are constantly transferred between the trapped states and the mobile states in the deposited fiber. When the charges are in the mobile states, they move rapidly toward the substrate. Therefore, the charges distribution of the earlier deposited layers has a lower peak value and is shifted closer to the

TABLE I. The parameters of the charge transport model.

Physical meaning	Parameter	Value
Distance	L	$300 \mu\text{m}$
Voltage	Φ	187.5 V
Height of the fiber	h	$2 \mu\text{m}$
Charge constant	ρ_0	$1 \times 10^{12} \mu\text{m}^{-1}$
Width of the Gaussian	w	$0.5 \mu\text{m}$
Standard deviation of the Gaussian	σ	$0.2 \mu\text{m}$
Charge mobility in PEO	μ	$1 \times 10^{-5} \text{ cm}^2 \text{ V}^{-2} \text{ s}^{-1}$
Charge diffusivity in PEO	D	$5 \text{ cm}^2 \text{ s}^{-1}$
Permittivity of PEO	ϵ_{peo}	5
Rate of charge transfer from the mobile state to the trapped state	$R_{f \rightarrow t}$	$2 \times 10^{-3} \text{ ms}^{-1}$
Rate of charge transfer from the trapped state to the mobile state	$R_{t \rightarrow f}$	$2 \times 10^{-3} \text{ ms}^{-1}$
Density of the trapped state	N_t	$1 \times 10^{12} \mu\text{m}^{-1}$

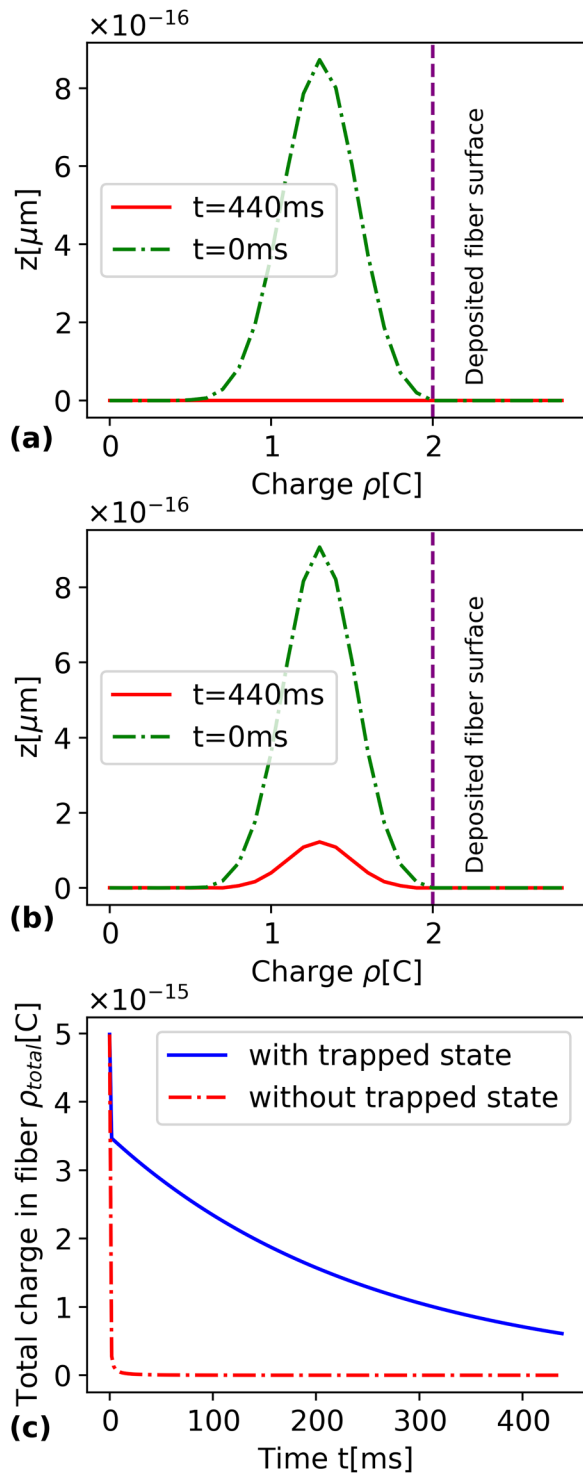


FIG. 2. The charge distribution of the deposited fiber (a) without the trapped state and (b) with the tapping state at $t = 0$ ms and $t = 440$ ms and (c) the change of total charges inside the deposited fiber over time.

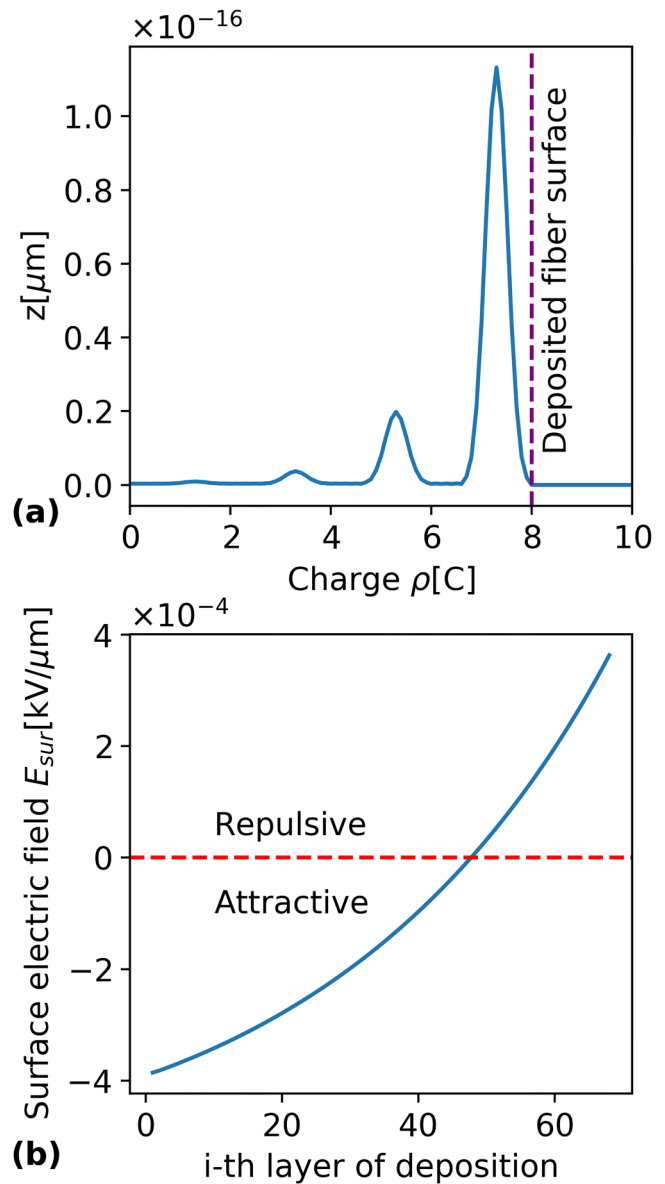


FIG. 3. (a) The charge distribution inside the four deposited polymer fibers at 2200 ms and the electric field at the surface of deposited wall before the deposition of the i th layer of polymer fiber.

substrate $z = 0$ as more charges have been transferred from the trapped to the mobile states. Moreover, the charge density at the interface between the deposited layer and the substrate $z = 0$ is non-zero, indicating that some charges accumulate along the interface.

Figure 3(b) depicts the surface electric field E_{sur} before the deposition of the i th layer, i.e., $i = 1, 2, 3$. When there are only a few layers, the surface E-field is negative, where the in-flight fiber is

31 January 2024 16:30:28

attracted by the deposited fiber. Even though the positive residual charges remain inside the deposited fiber, the dielectric property of the polymeric material shields the charges inside. Therefore, the electrostatic force enables stacking the positively charged in-flight fibers on top of the wall structure, a process known as self-alignment stacking,³² where the nanofibers form an organized structure among themselves without external direction. When the number of layers increases, more residual charges accumulate inside the deposited fiber as the charges dissipate slower than the charge added by the fiber deposition. As a result, the surface E-field increases with the number of deposited layer. After a certain number of layers, the dielectric medium can no longer shield all residual charge and the surface E-field eventually becomes positive, where the in-flight polymer fiber is repelled by the wall structure. The self-alignment of the fiber deposition breaks down, and the polymer fibers are unable to stack smoothly on top of the wall structure, limiting the control of the printing. According to the simulation results, the first layer with positive surface E-field, which we refer to as the breakdown layer in this work, is 49.

C. Effect of the substrate

In most NFES setups, the substrate is a different material than the polymer fiber. Due to the material mismatch, the charges in the polymer medium have to overcome a material-dependent energy barrier to transport to the substrate via an injection mechanism. In order to include the effect of the substrate, we introduce an energy barrier at the interface between the deposited fibers and the substrate by implementing a boundary condition for the current in Eq. (10). In the following, we analyze the effect of the different substrate materials on the charge dissipation. We use the same system as in Sec. III B and introduce the current boundary condition at $z = 0$ with an energy barrier ranging from 0 to 0.9 eV at 300 K. When there is no energy barrier, i.e., $\Delta = 0$ eV, the system is equivalent to the system in Sec. III B.

The charge distributions in the wall structure with energy barriers of $\Delta = 0, 0.1,$ and 0.2 eV at $t = 2200$ ms are shown in Fig. 4(a). For the systems with a non-zero energy barrier, the charge density is high around the region along the interface $z = 0$. Since only the charges with sufficient energy can pass through the energy barrier, the remaining charges are trapped and accumulate along the interface between the deposited fibers and the substrate. We find that the curve $\Delta = 0.2$ eV has a higher charge density than the curve $\Delta = 0.1$ eV at the interface. This is because fewer charges can pass through the energy barrier when the height of the barrier increases, causing more charges to accumulate along the interface.

Figure 4(b) depicts the breakdown layer of the fiber deposition with varying the energy barrier, while Fig. 4(c) depicts the surface E-field before the deposition of the 20th layer with varying the energy barrier. When there is no energy barrier, i.e., $\Delta = 0$, the breakdown layer of the self-alignment is 49, as discussed in Sec. III B, and the surface E-field is the most negative. As the dielectric medium can shield the accumulated charges, a slight increase in the barrier, i.e., $\Delta = 0.1$ eV, has little impact on the breakdown layer and the surface E-field. When the energy barrier rises further, there is a clear decrease in the breakdown layer and an increase in the surface E-field. This is due to the fact that more charges

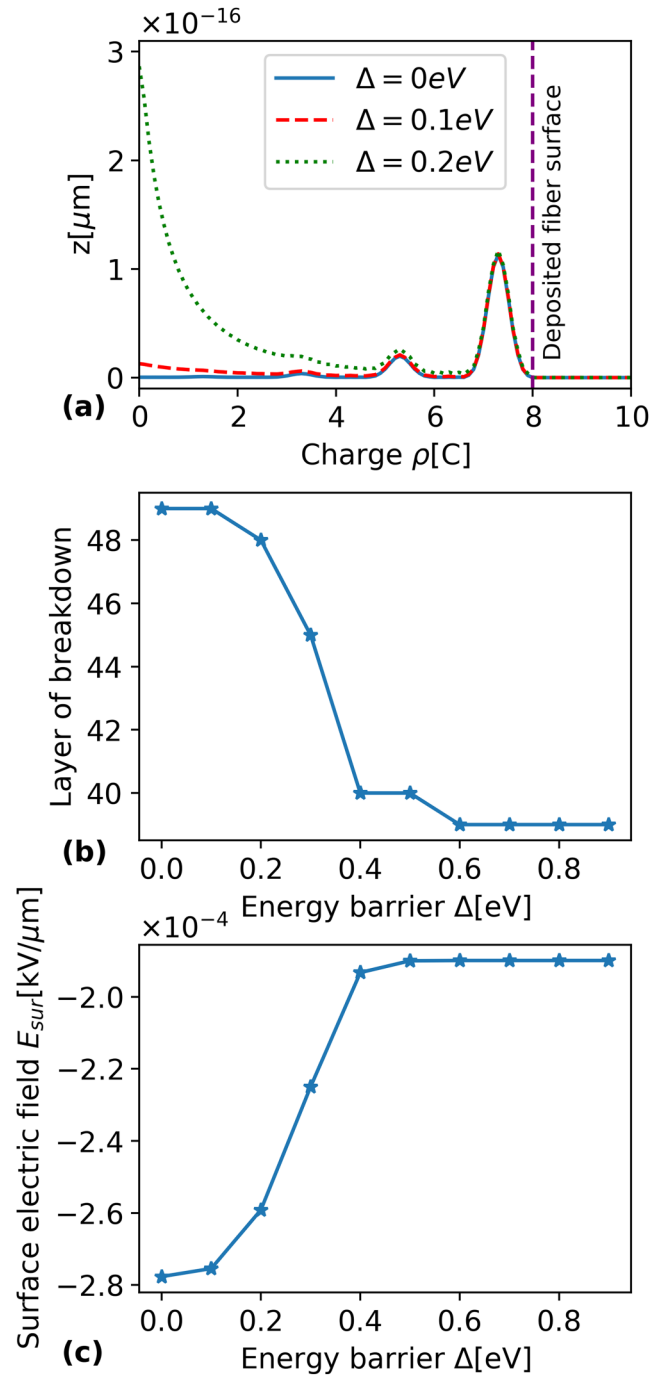


FIG. 4. (a) The charge distribution inside the wall structure with different energy barriers at $t = 2200$ ms, (b) the layer of breakdown with varying the height of energy barrier, and (c) the surface electric field of the wall structure at $t = 8800$ ms (before the deposition of the 20th layer) with varying the height of the barrier. (d) The experimental results of the aspect ratio with different substrate materials. (e)–(g) show the scanning electron microscope (SEM) images of the wall structure using SiO_2 , Si, and Ar/Cu as the substrate, respectively.³⁷

31 January 2024 16:30:28

accumulate at the interface and the dielectric medium cannot shield all residual charges. The inner residual charges can, thus, contribute to the electric field at the surface of the wall structure, hindering the self-alignment of the fiber deposition. Further increase in the energy barrier has a minor impact on the breakdown layer and the surface E-field, as the energy barrier is too high for all charges to pass through. As a result, increasing the energy barrier above a certain value has little effect on the breakdown layer and the surface E-field.

D. Effect of fiber materials and experimental parameters

To understand the effect of fiber materials and experimental parameters on the fiber deposition, we performed simulations with varying different model parameters. In the model, the fiber material is characterized by various parameters, including permittivity and mobility of the charge carriers in the fiber material, while the experimental parameters such as printing speed has also significant influence on the printing quality. Here, we consider the same systems as in Sec. III C with energy barrier of $\Delta=0.4\text{eV}$ and we computed the surface electric field of the deposited structure before the 20th layer deposition with varying model parameters, e.g., permittivity, mobility of the charge carriers, and printing speed.

The result of the surface electric field with varying mobility of the charge carriers in fiber is presented in Fig. 5(a). With low mobility, the charges are transported at a low speed in fiber. Increasing the mobility, the charges are transported at a higher speed. Therefore, more charges are dissipated during fiber deposition and the surface electric field decreases with increasing mobility.

Figure 5(b) shows the surface electric field with varying permittivity of the fibers. Dielectric material with high permittivity is able to polarize and shield to residue charges inside the material. The higher permittivity of the fiber materials implies more residue charges can be shielded by the deposited fiber. As a result, increasing the permittivity leads to the decrease of the surface electric field of the deposited structure.

The result of surface electric field with varying printing speed is depicted in Fig. 5(c). Printing speed corresponds to the rate of deposition of the next layer of fiber. The higher printing speed implies a shorter time for the deposition of the next layer of fiber, where the residue charges in the fibers have less time to dissipate before the next deposition. Therefore, increasing the printing speed hinders the charge dissipation and leads to an increase of the surface electric field.

E. Experimental validation

In order to validate our simulation result, we measure an aspect ratio which is a ratio of the height to the thickness of the wall structure formed by the deposited fiber in experiment. The aspect ratio is usually used to quantify the controllability of fiber deposition. Figure 6(a) shows the experimental results of aspect ratio with increasing number of deposited layers. When there are few layers in the wall structure, the aspect ratio gradually increases, indicating that the fibers are deposited in a self-aligned manner. After 80 layers, the aspect ratio decreases, implying that

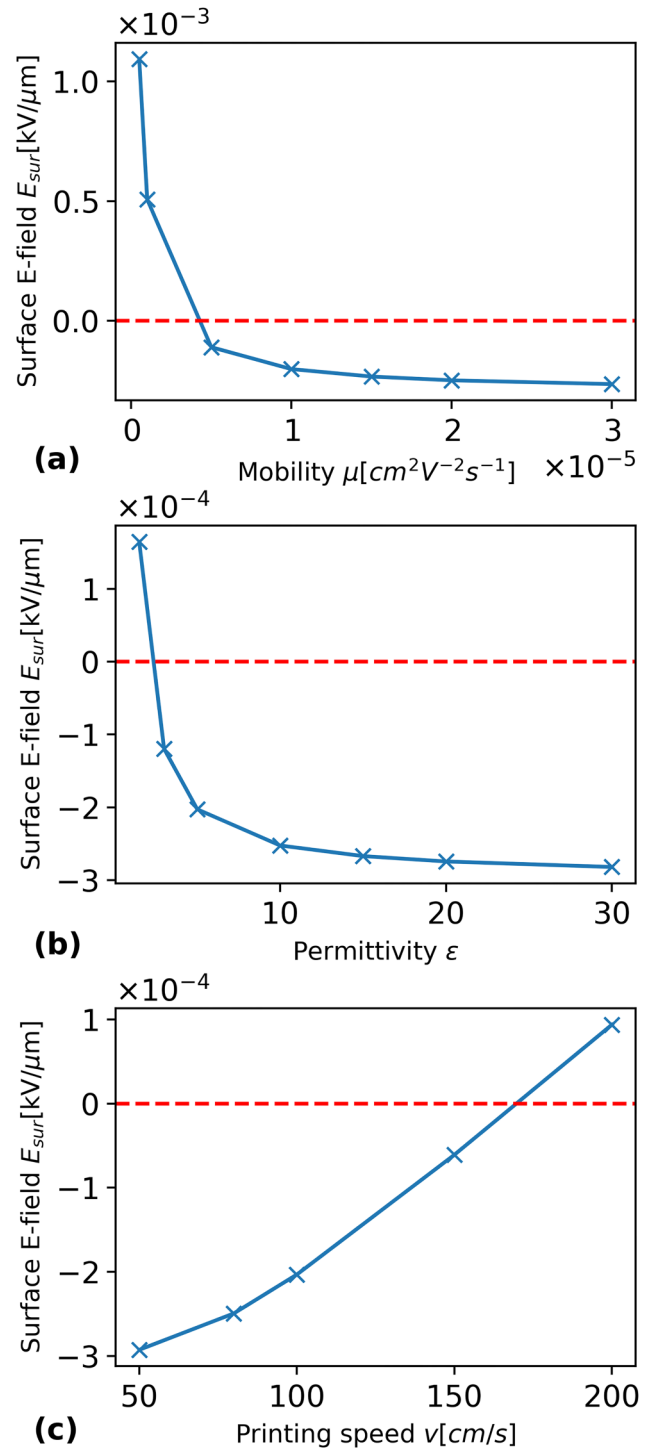


FIG. 5. The surface electric field of the deposited fibers at $t = 8800$ ms (before the deposition of the 20th layer) with varying (a) the mobility of the charge carriers in the fiber material, (b) the permittivity of the fiber material, and (c) the printing speed.

31 January 2024 16:30:28

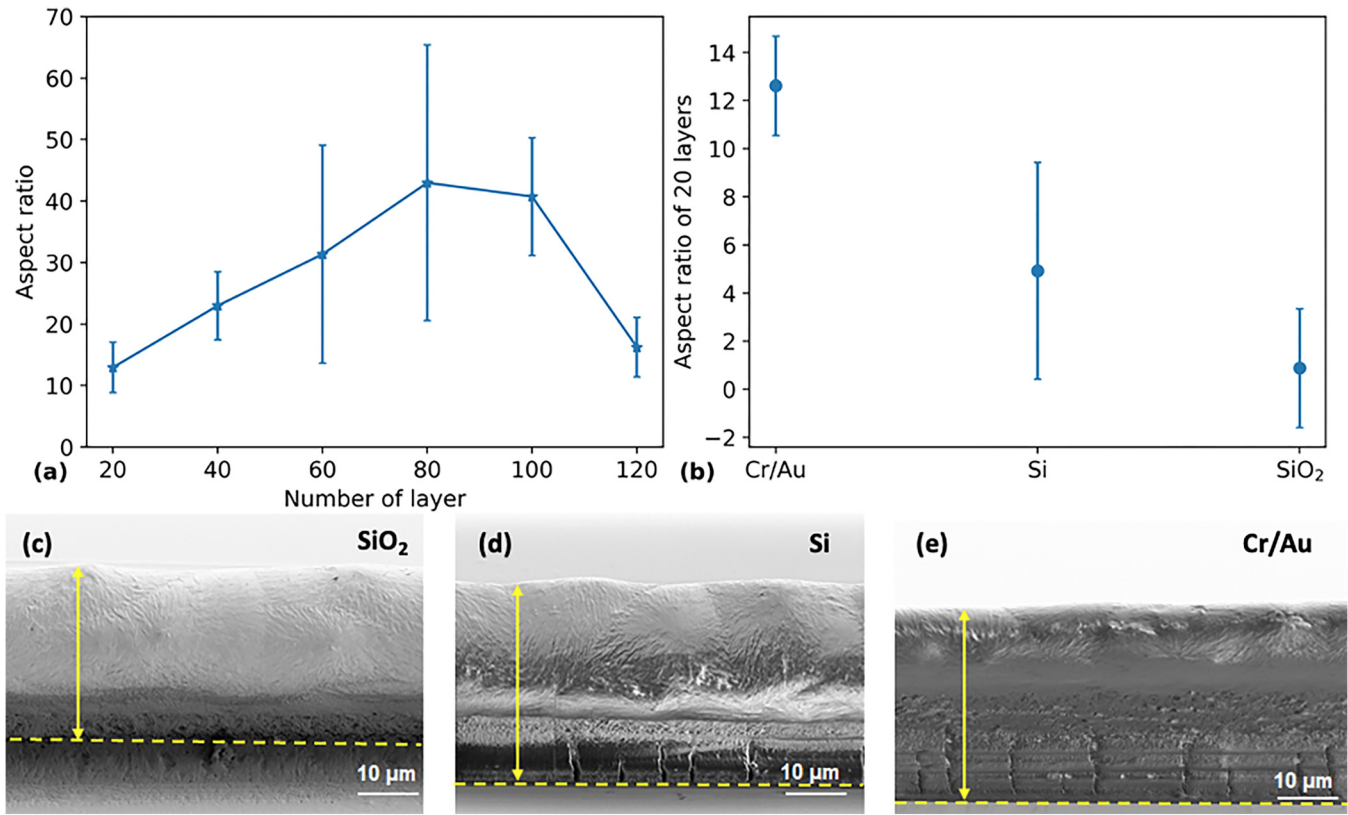


FIG. 6. (a) The aspect ratio of the wall structure with the number of deposited layers, (b) the aspect ratio of 20 layers structure deposited with different substrate material, (c)–(e) show the scanning electron microscope (SEM) images of the wall structure using SiO₂, Si and Ar/Cu as the substrate, respectively [reproduced with permission from A. Sadaf, *Adv. Eng. Mater.* **24**, 2101740 (2022). Copyright 2022, Author(s), licensed under a Creative Commons Attribution (CC BY) license], in which the yellow arrows indicate the height of the deposited fibers and the yellow dotted lines indicate the surface of the substrate.

31 January 2024 16:30:28

the self-alignment breaks down. By comparing the simulation results (>49 layers) to the experimental results (>80 layers), the simulation qualitatively agrees with the experiment by demonstrating the breakdown of the self-alignment mechanism.

Furthermore, we measure the aspect ratio of the structure with 20 layers on three different substrate materials, i.e., SiO₂, Si, and Cr/Au, and compare them with the simulation results. The scanning electron microscope (SEM) images of the structures of 20 layers stacked fibers on various substrate materials, i.e., (i) insulator (SiO₂), (ii) semiconductor (Si), and (iii) conductor (Cr/Au), are shown in Fig. 6(b)–6(e), respectively. For the conductor substrate, the charges are injected from the polymer medium to the conduction band of the conductive material, where they can be easily transported away from the substrate. As a result, the conductor substrate is equivalent to the system without an energy barrier and has the best aspect ratio among all substrates. For the semiconductor and the insulator substrates, the charges are transported from the polymer to the substrate via the hopping mechanism. This requires sufficient energy to activate the charge transport process, which corresponds to the system with an energy barrier. Therefore,

in the experiment, the semiconductor/insulator substrate has a lower aspect ratio because less charges have sufficient energy to overcome the energy barrier and the residue charges accumulate along the interface. This also shows a qualitative agreement with the simulation results in Sec. III C, in which substrate materials with lower energy barrier for charge injection show better deposition results.

IV. CONCLUSIONS

We presented a numerical model to simulate the charge transport, dissipation, and accumulation inside the polymeric fiber in NFES. We discussed a one-dimensional charge transport model in dielectric material in which the coupled transport equation, continuity equation, and Poisson equation are solved to model the dynamics of charge in the solidified electrospun fibers under an external electric field. To simulate the fiber deposition, a charged fiber segment is attached on top of the surface of the deposited fiber structure in each deposition cycle. The electromechanical behavior of the charged fiber deposition is studied by computing the surface electric field of the wall structure.

In the simulation, we compared the charge dissipation in the system with and without trapped states of the charge carriers, illustrating that trapped states are the main source of slow charge dissipation in the polymeric material. When the charge added by the fiber deposition is faster than the charge dissipation at the substrate, the residual charges in the deposited fibers accumulate. These residual charges contribute to the electric field at the surface of the wall structure and influence the electric interaction between the in-flight fiber and the deposited fibers. After a certain number of deposited layers, the electric force changes from attractive to repulsive, and the self-alignment of the fiber deposition eventually breaks down. In addition, an energy barrier at the interface between the deposited fibers and the substrate is introduced in the model to illustrate how different substrate materials affect the fiber deposition. When the energy barrier is low, most of the charges from the polymer fiber can be transported to the substrate, and only a few charges accumulate along the interface. When the energy barrier is high, a large number of charges do not possess sufficient energy to overcome it, causing them to accumulate along the interface region and hinder the self-alignment. The simulation results are in good qualitative agreement with the experiment results. We also tested various model parameters, such as mobility of charge carriers, permittivity, and printing speed, to analyze their effect on the printing quality. There are a few issues that would be worthwhile to investigate in the future in order to further study the fiber deposition in NFES. First, we assume that charge transport to the substrate is the only source of charge dissipation. However, charges in polymer fibers can also dissipate by solvent evaporation. Second, fiber deposition is also influenced by factors not considered here, such as the gravity and the movement of the collector.

In summary, we developed a model to study the mechanism of charged fiber deposition in near-field electrospinning. We also provide a in-depth analysis of the factors that influence the control of the electrospun direct-writing, i.e., the speed of deposition and the choice of substrate materials. With this newly developed model, we can analyze and evaluate the effect of the experimental parameters in order to minimize the charge accumulation in the polymer fiber to optimize the nanofiber deposition of the near-field electrospinning.

ACKNOWLEDGMENTS

This research has been funded by Deutsche Forschungsgemeinschaft (DFG, German Research Foundation) under Germany's Excellence Strategy for the Excellence Cluster "3D Matter Made to Order" (Grant No. EXC-2082/1-390761711) and by the Carl Zeiss Foundation. This work was performed on the HoreKa supercomputer funded by the Ministry of Science, Research and the Arts Baden-Württemberg and by the Federal Ministry of Education and Research.

AUTHOR DECLARATIONS

Conflict of Interest

The authors have no conflicts to disclose.

Author Contributions

Ka Chun Chan: Investigation (lead); Methodology (lead); Software (lead); Writing – original draft (lead); Writing – review & editing (lead). **Ahsana Sadaf:** Validation (supporting); Writing – review & editing (supporting). **Jan Gerrit Korvink:** Conceptualization (supporting); Writing – review & editing (supporting). **Wolfgang Wenzel:** Conceptualization (lead); Supervision (lead); Writing – review & editing (supporting).

DATA AVAILABILITY

The data that support the findings of this study are available from the corresponding author upon reasonable request.

REFERENCES

- I. Liashenko, J. Rosell-Llompart, and A. Cabot, "Ultrafast 3D printing with sub-micrometer features using electrostatic jet deflection," *Nat. Commun.* **11**, 753 (2020).
- A. Zolfaghari, T. Chen, and A. Y. Yi, "Additive manufacturing of precision optics at micro and nanoscale," *Int. J. Ext. Manuf.* **1**, 012005 (2019).
- B. Zhang, J. He, X. Li, F. Xu, and D. Li, "Micro/nanoscale electrohydrodynamic printing: From 2D to 3D," *Nanoscale* **8**, 15376–15388 (2016).
- A. Sola, A. Trinchi, and A. J. Hill, "Self-assembly meets additive manufacturing: Bridging the gap between nanoscale arrangement of matter and macroscale fabrication," *Smart Mater. Manuf.* **1**, 100013 (2023).
- D. Engstrom, B. Porter, M. Pacios, and H. Bhaskaran, "Additive nanomanufacturing—A review," *J. Mater. Res.* **29**, 1792–1816 (2014).
- X. Sui, J. R. Downing, M. C. Hersam, and J. Chen, "Additive manufacturing and applications of nanomaterial-based sensors," *Mater. Today* **48**, 135–154 (2021).
- X. Ruan, Y. Wang, N. Cheng, X. Niu, Y.-C. Chang, L. Li, D. Du, and Y. Lin, "Emerging applications of additive manufacturing in biosensors and bioanalytical devices," *Adv. Mater. Technol.* **5**, 2000171 (2020).
- A. Ahmed, I. Hassan, A. M. Pourrahimi, A. S. Helal, M. F. El-Kady, H. Khassaf, and R. B. Kaner, "Toward high-performance triboelectric nanogenerators by engineering interfaces at the nanoscale: Looking into the future research roadmap," *Adv. Mater. Technol.* **5**, 2000520 (2020).
- M. Sahu, S. Hajra, H.-G. Kim, H.-G. Rubahn, Y. Kumar Mishra, and H. J. Kim, "Additive manufacturing-based recycling of laboratory waste into energy harvesting device for self-powered applications," *Nano Energy* **88**, 106255 (2021).
- Y. Wang, M. Gao, D. Wang, L. Sun, and T. J. Webster, "Nanoscale 3D bio-printing for osseous tissue manufacturing," *Int. J. Nanomedicine* **15**, 215–226 (2020).
- M. Islam, A. D. Lantada, D. Mager, and J. G. Korvink, "Carbon-based materials for articular tissue engineering: From innovative scaffolding materials toward engineered living carbon," *Adv. Healthcare Mater.* **11**, 2101834 (2022).
- J. A. Smith and E. Mele, "Electrospinning and additive manufacturing: Adding three-dimensionality to electrospun scaffolds for tissue engineering," *Front. Bioeng. Biotechnol.* **9**, 674738 (2021).
- M. Altissimo, "E-beam lithography for micro-/nanofabrication," *Biomicrofluidics* **4**, 026503 (2010).
- V. Hahn, P. Kiefer, T. Frenzel, J. Qu, E. Blasco, C. Barner-Kowollik, and M. Wegener, "Rapid assembly of small materials building blocks (voxels) into large functional 3D metamaterials," *Adv. Funct. Mater.* **30**, 1907795 (2020).
- V. G. Rocha, E. Saiz, I. S. Tirichenko, and E. García-Tuñón, "Direct ink writing advances in multi-material structures for a sustainable future," *J. Mater. Chem. A* **8**, 15646–15657 (2020).
- D. Behera and M. Cullinan, "Current challenges and potential directions towards precision microscale additive manufacturing—Part I: Direct ink writing/jetting processes," *Precis. Eng.* **68**, 326–337 (2021).

- ¹⁷D. H. Reneker and A. L. Yarin, "Electrospinning jets and polymer nanofibers," *Polymer* **49**, 2387–2425 (2008).
- ¹⁸J. Xue, T. Wu, Y. Dai, and Y. Xia, "Electrospinning and electrospun nanofibers: Methods, materials, and applications," *Chem. Rev.* **119**, 5298–5415 (2019).
- ¹⁹A. L. Yarin, S. Koombhongse, and D. H. Reneker, "Taylor cone and jetting from liquid droplets in electrospinning of nanofibers," *J. Appl. Phys.* **90**, 4836–4846 (2001).
- ²⁰D. H. Reneker, A. L. Yarin, H. Fong, and S. Koombhongse, "Bending instability of electrically charged liquid jets of polymer solutions in electrospinning," *J. Appl. Phys.* **87**, 4531–4547 (2000).
- ²¹M. Lauricella, S. Succi, E. Zussman, D. Pisignano, and A. L. Yarin, "Models of polymer solutions in electrified jets and solution blowing," *Rev. Mod. Phys.* **92**, 035004 (2020).
- ²²M. Lauricella, F. Cipolletta, G. Pontrelli, D. Pisignano, and S. Succi, "Effects of orthogonal rotating electric fields on electrospinning process," *Phys. Fluids* **29**, 082003 (2017).
- ²³M. Lauricella, D. Pisignano, and S. Succi, "Three-dimensional model for electrospinning processes in controlled gas counterflow," *J. Phys. Chem. A* **120**, 4884–4892 (2016).
- ²⁴D. Sun, C. Chang, S. Li, and L. Lin, "Near-field electrospinning," *Nano Lett.* **6**, 839–842 (2006), pMID: 16608294.
- ²⁵X.-X. He, J. Zheng, G.-F. Yu, M.-H. You, M. Yu, X. Ning, and Y.-Z. Long, "Near-field electrospinning: Progress and applications," *J. Phys. Chem. C* **121**, 8663–8678 (2017).
- ²⁶J.-U. Park, M. Hardy, S. J. Kang, K. Barton, K. Adair, D. K. Mukhopadhyay, C. Y. Lee, M. S. Strano, A. G. Alleyne, J. G. Georgiadis, P. M. Ferreira, and J. A. Rogers, "High-resolution electrohydrodynamic jet printing," *Nat. Mater.* **6**, 782–789 (2007).
- ²⁷G. S. Bisht, G. Canton, A. Mirsepassi, L. Kulinsky, S. Oh, D. Dunn-Rankin, and M. J. Madou, "Controlled continuous patterning of polymeric nanofibers on three-dimensional substrates using low-voltage near-field electrospinning," *Nano Lett.* **11**, 1831–1837 (2011), pMID: 21446719.
- ²⁸J. Deng, C. Liu, and M. Madou, "Ultra-thin carbon nanofibers based on graphitization of near-field electrospun polyacrylonitrile," *Nanoscale* **12**, 10521–10531 (2020).
- ²⁹D. George, A. Garcia, Q. Pham, M. R. Perez, J. Deng, M. T. Nguyen, T. Zhou, S. O. Martinez-Chapa, Y. Won, C. Liu, R. C. Lo, R. Ragan, and M. Madou, "Fabrication of patterned graphitized carbon wires using low voltage near-field electrospinning, pyrolysis, electrodeposition, and chemical vapor deposition," *Microsyst. Nanoeng.* **6**, 7 (2020).
- ³⁰F. Ruggieri, D. Di Camillo, L. Lozzi, S. Santucci, A. De Marcellis, G. Ferri, L. Giancaterini, and C. Cantalini, "Preparation of nitrogen doped TiO₂ nanofibers by near field electrospinning (NFES) technique for NO₂ sensing," *Sens. Actuators B Chem.* **179**, 107–113 (2013).
- ³¹Z. Lou, X. Yang, H. Chen, and Z. Liang, "Flexible ultraviolet photodetectors based on ZnO–SnO₂ heterojunction nanowire arrays," *J. Semicond.* **39**, 024002 (2018).
- ³²G. Luo, K. S. Teh, Y. Liu, X. Zang, Z. Wen, and L. Lin, "Direct-write, self-aligned electrospinning on paper for controllable fabrication of three-dimensional structures," *ACS Appl. Mater. Interfaces* **7**, 27765–27770 (2015), pMID: 26592741.
- ³³G. Zheng, W. Li, X. Wang, D. Wu, D. Sun, and L. Lin, "Precision deposition of a nanofibre by near-field electrospinning," *J. Phys. D: Appl. Phys.* **43**, 415501 (2010).
- ³⁴G. Zheng, J. Jiang, X. Wang, W. Li, Z. Yu, and L. Lin, "High-aspect-ratio three-dimensional electrospinning via a tip guiding electrode," *Mater. Des.* **198**, 109304 (2021).
- ³⁵L. H. Catalani, G. Collins, and M. Jaffe, "Evidence for molecular orientation and residual charge in the electrospinning of poly(butylene terephthalate) nanofibers," *Macromolecules* **40**, 1693–1697 (2007).
- ³⁶Y.-S. Park, J. Kim, J. M. Oh, S. Park, S. Cho, H. Ko, and Y.-K. Cho, "Near-field electrospinning for three-dimensional stacked nanoarchitectures with high aspect ratios," *Nano Lett.* **20**, 441–448 (2020), pMID: 31763856.
- ³⁷A. Sadaf, M. Elter, D. Mager, U. H. F. Bunz, M. Islam, and J. G. Korvink, "Wall microstructures of high aspect ratio enabled by near-field electrospinning," *Adv. Eng. Mater.* **24**, 2101740 (2022).
- ³⁸J. M. Alison and R. M. Hill, "A model for bipolar charge transport, trapping and recombination in degassed crosslinked polyethylene," *J. Phys. D: Appl. Phys.* **27**, 1291 (1994).
- ³⁹I. Al-Dhahir, R. Kealy, S. Kelly, M. Yu, S. McNab, K. Collett, J. Liu, C. Grovenor, P. R. Wilshaw, and R. S. Bonilla, "Electrostatic tuning of ionic charge in SiO₂ dielectric thin films," *ECS J. Solid State Sci. Technol.* **11**, 063010 (2022).
- ⁴⁰S. L. Roy and M. Q. Hoang, "A bipolar charge transport model to simulate the impact of nanometric scale processes on the space charge behaviour in polyethylene," *J. Phys. D: Appl. Phys.* **55**, 465303 (2022).
- ⁴¹F. Boufayed, G. Teyssède, C. Laurent, S. Le Roy, L. A. Dissado, P. Ségur, and G. C. Montanari, "Models of bipolar charge transport in polyethylene," *J. Appl. Phys.* **100**, 104105 (2006).
- ⁴²X. Cai, X. Lin, J. Yu, and Z. Lu, "Modeling of space charge dynamics in polyethylene under ac stress based on bipolar charge transport model," *Mater. Res. Express* **7**, 115305 (2020).
- ⁴³G. Collins, J. Federici, Y. Imura, and L. H. Catalani, "Charge generation, charge transport, and residual charge in the electrospinning of polymers: A review of issues and complications," *J. Appl. Phys.* **111**, 044701 (2012).
- ⁴⁴A. Thyssen, K. Almdal, and E. V. Thomsen, "Electret stability related to the crystallinity in polypropylene," *IEEE Trans. Dielectr. Electr. Insul.* **24**, 3038–3046 (2017).
- ⁴⁵A. Mishra, "Studies of polymer electrets. II. Factors governing the stabilities of homoelectrets obtained from polystyrene and its derivatives," *J. Appl. Polym. Sci.* **27**, 1107–1118 (1982).
- ⁴⁶N. Mohmeyer, N. Behrendt, X. Zhang, P. Smith, V. Altstädt, G. M. Sessler, and H.-W. Schmidt, "Additives to improve the electret properties of isotactic polypropylene," *Polymer* **48**, 1612–1619 (2007).